I&EC research
Industrial & Engineering Chemistry Research

Article

pubs.acs.org/IECR

Enhancing the Crystal Production Rate and Reducing Polydispersity in Continuous Protein Crystallization

Joseph Sang-II Kwon,[†] Michael Nayhouse,[†] Gerassimos Orkoulas,[†] and Panagiotis D. Christofides*[,†,‡]

[†]Department of Chemical and Biomolecular Engineering and [‡]Department of Electrical Engineering, University of California, Los Angeles, California 90095, United States

ABSTRACT: This article focuses on the modeling and control of a continuous crystallizer with a fines trap and a product classification unit employed to produce tetragonal hen-egg-white lysozyme crystals. A kinetic Monte Carlo model is initially developed to simulate the crystal nucleation, growth, and aggregation processes taking place in the crystallizer using experimentally determined rate expressions. Subsequently, the influence of varying (a) the flow rates of the streams to the fines trap and the product classification unit and (b) the corresponding cutoff sizes is studied, and as a result, an operating strategy that takes advantage of the aggregation, fines removal, and product classification units is proposed to simultaneously achieve a high production rate and a low polydispersity of the crystals produced by the crystallizer. Finally, a model predictive controller is designed using a reduced-order model, which manipulates the jacket temperature to lead to the production of crystals with the desired shape and size distributions.

INTRODUCTION

The pharmaceutical industry is a key sector of the U.S. and global economy. In the pharmaceutical industry, protein crystallization plays a key role in relation to separation and purification methods for the production of drugs. Once a drug has been approved by the U.S. Food and Drug Administration (FDA), the patent of the drug will prevent other companies from manufacturing and selling drugs with the exact same ingredients until the patent expires. Because of the fact that significant financial investment as well as time is required for the discovery of a new drug, a pharmaceutical company generally files a patent even before the clinical trial in order to protect its intellectual property. As a result, after a company enters the market with a new drug, it has only a limited period to make significant profit. Therefore, companies look for ways to maximize their revenues for the limited monopoly period. In an effort to find a win−win situation for both the patent holders and consumers (e.g., patients), significant research efforts have focused on the modeling and control of crystallization processes to further improve the production rate and quality of the crystal products in the manufacturing process, aiming at providing higher revenues to the companies and affordable prices to the customers.[1,2] Specifically, Majumder and Nagy[3] presented a systematic approach to obtaining the optimal temperature profile in a continuous plug-flow reactor along with the consideration of dissolution through the fines trap process.

In many chemical processes including crystallizers, agitation of the particulate solution is required in order to maintain solid particles in the bulk of the suspension. In particular, two main suspension types are prevalent in industrial practice, namely, complete suspension and homogeneous suspension. More specifically, complete suspension is said to be achieved when all particles are lifted and no particle remains on the bottom of the crystallizer for more than 1−2 s.[4] When such a condition is achieved, the contact area between the crystals and fluid is maximized so that the entire surface area of the crystals is available for surface reactions and mass-transfer processes. Additionally, homogeneous suspension corresponds to the state of suspension at which the particle number concentration and size distributions are uniform throughout the crystallizer and a further increase in the stirrer speed does not significantly enhance the quality (i.e., uniformity) of the suspension. In general, the necessity of homogeneous suspension is mainly determined by the purpose of the crystallizer operation. For example, a homogeneous suspension is required when the stirred crystallizer plays a role as a mixer where the suspension must be fed into another processing unit. Furthermore, homogeneous suspension is often desired in the context of crystallization processes because nonuniform spatial distribution of crystals may lead to unacceptably high local supersaturation levels and thereby unexpectedly high crystal growth rates. Additionally, the occurrence of a homogeneous suspension will reduce the uncertainty in the online measurements of continuous crystallization process variables because a representative sample of crystal products will be required for the online measurements of the crystal size and shape distributions.

There have been a number of theoretical and experimental attempts to model the minimum stirrer speed N_{js}, which is required to achieve the complete suspension configuration. In particular, Zwietering[4] carried out a dimensional analysis of the important system parameters and suggested eq 1, which is a function of the impeller type, reactor size, reactor geometry, off-bottom clearance height, and physical properties:

Special Issue: Alírio Rodrigues Festschrift

Received: February 26, 2014
Revised: April 6, 2014
Accepted: April 7, 2014
Published: April 7, 2014

dx.doi.org/10.1021/ie5008163 | *Ind. Eng. Chem. Res.* 2014, 53, 15538−15548

$$N_{js} = S\left(\frac{g(\rho_S - \rho_L d_p)}{\rho_L}\right)^{0.45} \frac{\nu^{0.1} X^{0.13}}{d_p^{0.25} D^{0.85}} \quad (1)$$

where S is a dimensionless constant presented graphically as a function of the impeller type (e.g., paddles, six-bladed disk turbine, four-bladed disk turbine, vaned disk, propellers, and so on) and reactor geometry, d_p is the mean particle diameter, X is Zwietering's mass ratio percent (mass of solid/mass of liquid) × 100, D is the impeller diameter, g is the gravitational acceleration constant, ν is the kinematic viscosity, and ρ_L and ρ_S are the density of the continuous phase and crystals, respectively. The correlation is based on an assumption that the mixing energy required to suspend a particle equals the energy dissipated by the particle moving at its terminal velocity in a stagnant fluid.[5] Furthermore, it was proposed by Harnby et al.[6] and Baldi et al.[7] that the eddies that will lift particles from the bottom must be on the order of the size of the particles. For the case of mixing tanks with a six-bladed disk turbine, an empirical correlation was presented by Nienow.[8] However, the correlation proposed by Baldi et al.[7] is not used as much as the Zwietering correlation because it does not contain solids concentration and viscosity terms, which in general play a key role in describing the characteristics of a crystallizer. Lastly, the recent advances in the development of computational fluid dynamics have shed new light on the modeling of N_{js} in mechanically agitated vessels.[9]

The stirrer speed required to maintain the system in a homogeneous suspension is relatively high so that it will induce the formation of crystal aggregates. Specifically, an aggregate forms when two crystals collide with each other, and the resulting aggregate remains stable if it overcomes repulsive forces such as the hydrodynamic force due to the turbulent flow and viscous fluid layers between the two particles. Additionally, only binary aggregation is of interest in this work, and for the purpose of simulation, we adopt an assumption employed in our previous work that the shape of the crystal aggregate remains identical with that of the bigger crystal after an aggregation event occurs.[10] Particularly in the pharmaceutical industry, the aggregated crystal is desirable because it can accelerate the size enlargement process (i.e., typically this has been done through crystal growth only), which will, in turn, reduce the residence time required for crystals to grow to a desired crystal size. Through the aggregation process, many small crystal fines will be removed, and as a result, the production of crystals with a more uniform size distribution can be achieved, which will lead to uniform bio-availability of the crystal products.

In this work, we investigated the influences of varying the flow rates of the streams to the fines trap and the product classification unit and their cutoff sizes to the number concentration and size distribution of crystals inside the crystallizer, which will, in turn, affect the aggregation rate significantly. Therefore, an operating strategy that takes advantage of the aggregation process is proposed in order to achieve a high production rate and a low polydispersity (i.e., a narrow size distribution). Additionally, the shape distribution of the crystal aggregates is regulated to a desired value through a model predictive control (MPC) scheme.

The paper is organized as follows. Initially, a continuous crystallization process, involving a fines trap and a product classification unit, at a homogeneous suspension state is modeled through kinetic Monte Carlo (kMC) model methods in the way described in ref 11 using the rate equations originally developed by Durbin and Feher.[12] Specifically, the kMC simulation is employed to compute the net crystal growth rate accounting for the dependence of the detachment rate on the surface microconfiguration. Furthermore, the evolution of the crystal shape, which is represented by the ratio between the heights in the direction of the (110) and (101) faces, is modeled through the kMC simulation. Lastly, the kMC simulation can be used to predict the crystal growth dynamics at the operating conditions where experimental data are not available. Because kMC models are not readily available in a closed form, a population balance model is presented and the method of moments is applied to derive a reduced-order ordinary differential equation (ODE) model. Then, the ODEs are used for the design of an MPC scheme used to regulate the average shape of the crystal population to a desired value.[13,14]

DESCRIPTION AND MODELING OF THE CRYSTALLIZATION PROCESS

Process Description. We consider a continuous crystallizer where a fines trap is used to increase the average volume of the crystals inside the crystallizer by removing small crystal fines through a dissolution process such as a heat exchanger.[15] Additionally, a product classification unit is used to remove large crystals whose sizes are greater than the product cutoff size V_p through the product stream, while the small crystals are recycled back to the crystallizer to grow larger.[1,16] The configuration of the crystallizer used in this work is shown in Figure 1.

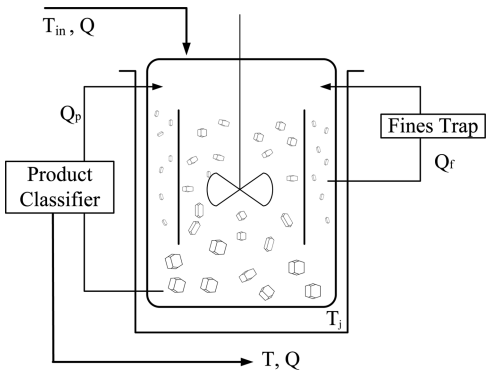

Figure 1. MSMPR crystallizer with a fines trap and a product classifier. T is the crystallizer temperature, T_i is the inflow temperature, T_j is the jacket temperature, Q is the flow rate of the inflow stream, and Q_p and Q_f are the flow rates of the streams to the product classifier and the fines trap, respectively.

The system parameters for the crystallizer considered in this work are taken from Smejkal et al.[17] and are presented as follows: A three-bladed propeller is considered for this work; the inner crystallizer diameter is T_d = 0.12 m; the crystallizer filling height is H = 0.12 m; the impeller height from the bottom of the crystallizer (i.e., the clearance height) is C_h = 0.04 m, and the impeller diameter is D = 0.06 m. Therefore, T_d/D and T_d/C_h were 2 and 3, respectively, and these variables are used to compute the dimensionless constant S in eq 1.

Crystal Nucleation and Growth. Typically, secondary nucleation plays a key role when the stirrer speed is sufficiently high that it induces crystal attrition or abrasion because of collision with a crystallizer wall, with a propeller, or with other crystals. For example, Tait et al.[18] presented that attrition is an

dx.doi.org/10.1021/ie5008163 | Ind. Eng. Chem. Res. 2014, 53, 15538−15548

important source of secondary nuclei formation in lysozyme crystallization. However, for the purpose of modeling and simulation of the effect of the aggregation process on the production rate, the degree of the attrition process resulting from a relatively high stirrer speed is disregarded. For the same reason, secondary nucleation, which is typically attributed to the attrition process, is ignored, and only primary nucleation of hen-egg-white (HEW) lysozyme crystals is considered in this work. Furthermore, there is another supporting reason for not accounting for secondary nucleation in that the impeller Reynolds number computed in the following section amounts to $Re_{imp} = 8.0 \times 10^3$, and according to Harnby et al.,[6] it is appropriate to assume that the degree of crystal attrition is negligible when $Re_{imp} < 10^4$. Additionally, the nucleated crystals are assumed to be of infinitesimal size.[10,19,20] The nucleation rate at 4% (w/v) NaCl and pH 4.5, $B(\sigma)$, is taken from ref 21 and is of the form

$$B(\sigma) = \begin{cases} 0.041\sigma + 0.063 & \text{for} \quad \sigma \geq 3.11 \\ 8.0 \times 10^{-8} \exp(4.725\sigma) & \text{for} \quad \sigma < 3.11 \end{cases} \tag{2}$$

with units #/cm^3 s. Although it does not look similar to a typical nucleation expression, this expression provides a valid nucleation rate. In this work, the relative supersaturation is defined as $\sigma = \ln(C/s)$ where C (mg/mL) is the current solute concentration in the continuous phase and the solubility s (mg/mL) is given as follows:[22,23]

$$s(T) = 2.88 \times 10^{-4}T^3 - 1.65 \times 10^{-3}T^2 + 4.62 \times 10^{-2}T + 6.01 \times 10^{-1} \tag{3}$$

Although this solubility equation is not the standard van't Hoff equation, it is taken from the literature[22,23] where the solubility data are validated through the experiments.

Once the size of a crystal nucleus exceeds a critical size limit, which is usually in the dimension of several tens of a nanometer, it starts to grow spontaneously through adsorption, migration, and desorption mechanisms. Empirical expressions have been widely used to simulate the crystal growth.[24] However, in this work, the kMC simulations are used for more realistic modeling of a continuous crystallization process. Specifically, in this work, the solid-on-solid model is adopted to avoid voids and overhangs, resulting in the crystallization of very compact crystals. Reflecting that no finite size effect is observed,[25] a square lattice model with 30 × 30 lattice sites is employed along with periodic boundary conditions. Furthermore, we take into consideration the effect of additional factors such as pH values, NaCl concentrations, salt ions attached to the protein molecule, liquid impurities and buffer solution included in the crystals, and so on.[26−29] The lysozyme molecules considered in the kMC simulations are assumed to be transported instantaneously to the vicinity of the crystal surface, and thus we only focused on the attachment, detachment, and migration precesses of the molecules near the surface. In order to simulate the crystal growth mechanism, the three rate equations of Table 1 are used in the kMC simulations.[12,25,30]

In Table 1, K_0^+ is the adsorption coefficient, i is the number of nearest neighbors, E_{pb} is the average binding energy per bond, and ϕ is the total binding energy when a molecule's bonds are fully occupied by neighboring molecules (i.e., when $i = 4$). The nearest neighbors of a lattice site explicitly considered in this work are on the (N, S, E, W) directions, which are of the same

Table 1. Crystal Growth Rate Equations

surface reaction	rate equations
adsorption r_a	$K_0^+ \exp(\sigma)$
desorption $r_d(i)$	$K_0^+ \exp[\phi/k_BT - i(E_{pb}/k_BT)]$
migration $r_m(i)$	$K_0^+ \exp[\phi/k_BT - i(E_{pb}/k_BT) + E_{pb}/2k_BT]$

height or higher compared to the current lattice site. A further description of this can be found in the previous work.[30]

When a crystal will enter the fines trap or product classification unit is determined by its residence time. Thus, the effect of back-mixing in the crystallization process is reflected in the kMC simulations by applying the residence time distributions for both the fines trap and product classification units. Specifically, both the fines trap and product classification unit are assumed to follow an exponential residence time distribution:[31]

$$\exp(-\tau_f/\overline{\tau}_f) = \text{RN1}$$

$$\exp(-\tau_p/\overline{\tau}_p) = \text{RN2}$$

where τ_f and τ_p are the residence times of a crystal until it enters the fines trap and product classification unit, respectively, and $\overline{\tau}_f$ and $\overline{\tau}_p$ are the mean residence times of the corresponding processes. Additionally, RN1 and RN2 are randomly generated numbers in the range of (0,1]. As soon as a crystal is formed ($t = 0$), two residence times, τ_f and τ_p, will be given to the crystal for the fines trap and product classification unit, respectively. When $t = \tau_f$ seconds, the crystal will enter the fines trap and will be either removed or recycled back to the crystallizer depending on its size. If the crystal survives, then it grows to a larger crystal and it enters the product classification unit when $t = \tau_p$ seconds. Similarly, the crystal will leave the crystallizer if it is greater than the cutoff size, while it will get a new residence time $\tau_{p'}$ and will further stay in the crystallizer unless it is sufficiently large. The crystal will continue to grow, and it will be checked again at $t = \tau_p + \tau_{p'}$. This process continues until the crystal reaches the product cutoff size.

One of the most widely used product classification units is the hydrocyclone, where a centrifugal force is generated by injecting the fluid tangentially into the device. Therefore, we can increase the product cutoff size as we decrease the centrifugal force generated by the device. Furthermore, the product cutoff size is determined by the characteristics of the inflow and the geometry of the hydrocyclone, and thus there is no constrained upper bound on the product cutoff size.

In general, if the mean residence time for the product classification unit, $\overline{\tau}_f$, increases, crystals will be checked less often than in the case with a smaller $\overline{\tau}_f$, and thus some crystals may leave the crystallizer with their sizes greater than the desired product cutoff size. As a result, the volume distribution of the crystals at the outlet of the crystallizer will be a broader distribution to the right. On the other hand, if $\overline{\tau}_f$ decreases, the production of crystals with a very narrow size distribution will be achieved.

Balance Equations. *Mass Balance.* The amount of the protein solute in the continuous phase is described by the following mass balance equation:

$$\frac{dC}{dt} = \underbrace{-\frac{\rho_c}{V_{MSMPR}}\frac{dV_{crystal}}{dt}}_{\text{removed via crystallization}} + \underbrace{\frac{C_0}{\tau}}_{\text{incoming flow}} + \underbrace{\frac{\rho_c}{V_{MSMPR}}\frac{dV_{fines}}{dt}}_{\text{added by fines trap}} - \underbrace{\frac{C}{\tau}}_{\text{outgoing flow}} \tag{4}$$

where C is the protein solute concentration in the continuous phase, C_0 and τ are the solute concentration and residence time

dx.doi.org/10.1021/ie5008163 | Ind. Eng. Chem. Res. 2014, 53, 15538−15548

of the fresh feed stream to the crystallizer, V_{MSMPR} is the crystallizer volume, $V_{crystal}$ is the total volume of the crystals in the crystallizer, and V_{fines} is the total volume of crystals dissolved through the fines trap. Furthermore, the first term accounts for the amount of solute transported from the continuous phase to the crystal surface. The second and third terms represent the amount of solute added through the incoming flow from a fresh feed solution and from the fines trap, respectively. Then, the last term indicates the amount of solute removed from the continuous phase through the product stream from the crystallizer.

Energy Balance. The crystallizer temperature is primarily adjusted through manipulation of the jacket temperature. Additionally, the temperature change due to the enthalpy of crystallization as well as heat transfer from the inflow/outflow is accounted for as follows:

$$\frac{dT}{dt} = -\frac{\rho_c \Delta H_c}{\rho C_p V_{MSMPR}} \frac{dV_{crystal}}{dt} - \frac{U_c A_c}{\rho C_p V_{MSMPR}}(T - T_j) + \frac{T_{in} - T}{\tau} \quad (5)$$

where T_{in} is the temperature of the incoming stream, T and T_j are the crystallizer and jacket temperatures, respectively, ρ_c = 1400 mg/cm^3, ΔH_c = −44.5 kJ/kg is the enthalpy of the reaction, ρ = (1000 + C) mg/cm^3, C_p = 4.13 kJ/K·kg is the specific heat capacity, V_{MSMPR} = 1 L is the volume of the crystallizer, A_c = 0.25 m^2 is the area of the crystallizer wall that is in contact with the jacket stream, and U_c = 500 kJ/m^2·h·K is the crystallizer wall's overall heat-transfer coefficient. For more details regarding the derivation of the balance equations above, please refer to refs 32 and 33 for the derivation of eqs 4 and 5.

Stirrer Speed in the Crystallizer. *Stirrer Speed Required for Complete Suspension N_{js}.* In 1958, Zwietering[4] suggested eq 1 to predict the minimum impeller speed, N_{js}, required to achieve complete suspension. Additionally, S values for five impeller types with different reactor geometries (e.g., T_d/C_h and T_d/D) are presented in refs 4 and 6 through graphs from which the value of S = 6.7 was evaluated. If no power curve is available for a specific reactor/impeller geometry of interest, experimental work should be done to construct a specific power curve for this geometry. Additionally, for non-Newtonian fluids, the apparent viscosity is determined from viscometric data at an appropriate shear rate and used directly in the usual Newtonian power number−Reynolds number correlation.[6] Lastly, the mass ratio percent X = 0.6% is computed by using the following expression:

$$X = 100 \times \frac{M_s}{\rho_L V_{MSMPR} - M_s}$$

where M_s is the mass of the crystals.

As a result, N_{js} = 4.87/s is obtained by using eq 1. Prior to computation of the power number N_p at the complete suspension speed N_{js} = 4.87/s, we evaluated the impeller Reynolds number Re_{imp} through the following expression:

$$Re_{imp} = \frac{\rho_L N_{js} D^2}{\mu}$$

where Re_{imp} = 8.0 × 10^3 was computed by implying that the system is fully turbulent and the corresponding N_p = 0.25 is read from a power curve.[34] Additionally, the power input P required by a motor in order to maintain the crystallizer in the complete suspension state is calculated through the following equation:[6]

$$P = N_p \rho_L N_{js}^3 D^5 \quad (6)$$

Then, the mean energy dissipation rate, $\bar{\varepsilon}_{js}$ = 0.025 W/kg, is obtained from the following expression[17] at the agitation speed N_{js}:

$$\bar{\varepsilon}_{js} = \frac{P}{\rho_L V_{MSMPR}} \quad (7)$$

Settling Velocity V_t. When the drag force balances the buoyancy and gravitational force acting on the crystal in a stagnant fluid, the settling velocity, V_t, of a crystal will be achieved. In an agitated crystallizer, it is difficult to clearly quantify a particle settling velocity because of the complexity in the solid suspension system. However, the particle settling velocity of a crystal in the agitated crystallizer is always less than the settling velocity in a stagnant fluid.[35] To this end, in Newtonian fluids, the free settling velocity, V_t, is calculated by the following expression:[36]

$$V_t = \sqrt{\frac{4 g d_p (\rho_S - \rho_L)}{3 C_D \rho_L}} \quad (8)$$

where the drag coefficient, C_D, is a function of the particle shape and the particle Reynolds number, Re_p, which is defined as follows:

$$Re_p = \frac{\rho_L V_t d_p}{\mu} \quad (9)$$

The correlation for C_D covers several hydrodynamic regimes.[36] In this work, it is assumed that the corresponding regime for this study is the Stokes' law (laminar) regime, where Re_p < 0.3 and the correlating expression for C_D is

$$C_D = \frac{24}{Re_p} \quad (10)$$

Note that using eqs 8−10 requires an iterative calculation because of the fact that the value of the particle Reynolds number determines the flow regime, which, in turn, determines which C_D expressions to use. On the other hand, to evaluate the particle Reynolds number, one needs the value of V_t. After several iterations, V_t = 1.9 × 10^{-3} m/s is obtained at Re_p = 0.11 and C_D = 204, which verifies that the system is in the laminar regime.

Agitation Speed for Homogeneous Suspension N_{hs}. In work by Paul et al.,[36] it was shown that a higher energy input is required to advance from complete suspension to homogeneous suspension. Specifically, for particles with a free settling velocity 5 × 10^{-4} m/s < V_t < 3 × 10^{-2} m/s, the power required to achieve homogeneous suspension is 2 times that required for complete suspension. As is shown by eq 7, the mean energy dissipation rate required to achieve homogeneous suspension is $\bar{\varepsilon}_{hs}$, and thus it follows that

$$\bar{\varepsilon}_{hs} = 2\bar{\varepsilon}_{js}$$

Aggregation Rate. We can compute the corresponding shear rate G_{shear} = 147.5/s required to achieve homogeneous suspension for the crystallizer considered in this work at $\bar{\varepsilon}_{hs}$ = 0.05 W/kg as follows:

dx.doi.org/10.1021/ie5008163 | Ind. Eng. Chem. Res. 2014, 53, 15538−15548

$$G_{shear} = \sqrt{\frac{\overline{\varepsilon}_{hs}}{\nu}}$$

We may also consider the maximum aggregation rate, which is determined by $G_{shear,max}$ = 1201/s at $\varepsilon_{max} = 72\overline{\varepsilon}_{hs}$ = 3.61 W/kg. Further details regarding ε_{max} can be found in a previous work.[15] Also, process parameters are presented in Table 2.

Table 2. Process Parameters

g	gravitational acceleration constant	9.8	m/s^2
ν	kinematic viscosity	2.3×10^{-6}	m^2/s
μ	dynamic viscosity	0.0024	kg/m·s
V_{MSMPR}	crystallizer volume	1	L

POPULATION BALANCE EQUATION (PBE)

PBE of the Crystal Volume Distribution. The dynamic evolution of the crystal volume distribution in a continuous crystallizer with a fines trap and a product classification unit accounting for nucleation, crystal growth, and aggregation is described as follows:

$$\frac{\partial n(V,t)}{\partial t} + G_{vol}\frac{\partial n(V,t)}{\partial V} = -\left[\underbrace{\frac{h(V-V_p)}{\tau_p}}_{product\ classifier} + \underbrace{\frac{1-h(V-V_f)}{\tau_f}}_{fines\ trap}\right] n(V,t) + \underbrace{\frac{1}{2}\int_0^V \alpha_{eff}\beta(V-\bar{V},\bar{V})n(V-\bar{V},t)n(\bar{V},t)d\bar{V}}_{Birth\ by\ aggregation} - \underbrace{n(V,t)\int_0^\infty \alpha_{eff}\beta(V,\bar{V})n(\bar{V},t)d\bar{V}}_{Death\ by\ aggregation} \quad (11)$$

with the following boundary condition:

$$n(0,\ t) = \frac{B(\sigma)}{G_{vol}}$$

where V and $V - \bar{V}$ are the crystal volumes, t is the time, α_{eff} is the aggregation efficiency, $\beta(V-\bar{V},\bar{V})$ is the aggregation rate for the crystals whose volumes are V and $V - \bar{V}$, τ_p and τ_f are the residence times for the streams to the product classification unit and fines trap, respectively, $n(V,t)$ is the number concentration of the crystals with volume V at time t, $B(\sigma)$ is the nucleation rate, and V_p and V_f represent the cutoff sizes for the product classification unit and fines trap, respectively. Then, a step function $h(V)$ is introduced as follows:

$$h(V) = \begin{cases} 1 & \text{for} \quad V \geq 0 \\ 0 & \text{for} \quad V < 0 \end{cases}$$

Furthermore, the volumetric growth rate of crystals, G_{vol}, is calculated as follows:

$$G_{vol}(t) = M_0(t)\left(2\frac{d\langle h_{110}\rangle}{dt}\langle h_{110}(t)\rangle\langle h_{101}(t)\rangle + \frac{d\langle h_{101}\rangle}{dt}\langle h_{110}(t)\rangle^2\right) + \frac{dM_0}{dt}\langle V(t)\rangle \quad (12)$$

where $\langle h_{110}\rangle$ and $\langle h_{101}\rangle$ are the average crystal heights in the direction of the (110) and (101) faces, as described in Figure 2, respectively, and M_0 is the number of crystals inside the crystallizer. Those three variables are obtained from the kMC simulation accounting for the fact that, in practice, they are estimated by the online measurements available through the focused beam reflectance measurement (FBRM) and process vision and measurement (PVM) in an experimental system.[15] To deal with the presence of intermittent measurements, the following moment models are used along with mass and energy balances to predict the dynamic evolution of the crystal volume and shape distributions during the period where the measurements are not available.

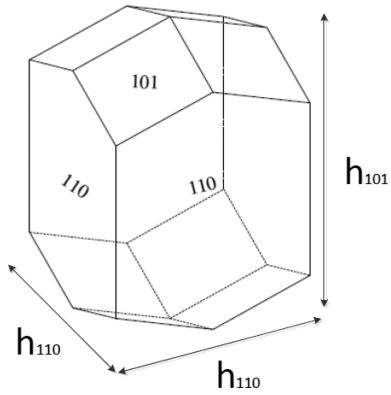

Figure 2. Morphology of a tetragonal HEW lysozyme crystal.

Moment Models. The computational cost of numerically solving eq 11 to obtain the crystal volume distribution is expensive and not immediately accessible in general because of the complexity of the PBE. To handle this issue, a reduced-order model is derived by applying the method of moments to eq 11. We define j^{th} moment as follows:

$$M_j = \int_o^\infty V^j n(V,\ t)\ dV \quad (13)$$

The following three moments and the balance equations are used to estimate the dominant behavior of the continuous crystallization process. For the derivation of the moment model, the reader may refer to refs 10 and 15.

Zeroth Moment. The dynamic evolution of the number of crystals is given by

$$\frac{dM_0}{dt} = B(\sigma) - \int_{V_p}^\infty \frac{n(V,\ t)}{\tau_p}\ dV - \int_0^{V_f} \frac{n(V,\ t)}{\tau_f}\ dV - \alpha_{eff}(M_0M_1 + 3M_{1/3}M_{2/3}) \quad (14)$$

where $B(\sigma)$ is from eq 11. The first integral term represents the number of crystal products larger than the cutoff size of the product classification unit, and the second integral term represents the number of small crystal fines removed through the fines trap. Both integral terms can be calculated from the online measurement, where the mean and standard deviation of the size and shape distributions are available. The last term corresponds to the decrease in the number of crystals due to the formation of aggregates, where α_{eff} is a constant collision efficiency and $M_{1/3}$ and $M_{2/3}$ are fractional moments.

First Moment. The dynamic evolution of the entire crystal volume is given by

$$\frac{dM_1}{dt} = G_{vol}M_0 - \int_{V_p}^\infty V\frac{n(V,\ t)}{\tau_p}\ dV - \int_0^{V_f} V\frac{n(V,\ t)}{\tau_f}\ dV \quad (15)$$

Second Moment. The dynamic evolution of the crystal volume square of the entire population is given by

dx.doi.org/10.1021/ie5008163 | Ind. Eng. Chem. Res. 2014, 53, 15538−15548

$$\frac{dM_2}{dt} = 2G_{vol}M_1 - \int_{V_p}^{\infty} V^2 \frac{n(V,t)}{\tau_p}\,dV - \int_0^{V_f} V^2 \frac{n(V,t)}{\tau_f}\,dV + 2\alpha_{eff}(M_1M_2 + 3M_{4/3}M_{5/3}) \quad (16)$$

The fines trap and product classification unit terms in the moment equations above can be numerically integrated because the online measurements of the mean and standard deviation of the crystal volume distribution are assumed to be available as discussed above.[15]

OPEN-LOOP SIMULATION RESULTS

In this work, the kMC simulation is used to model a continuous crystallization process with a fines trap and a product classification unit. The stirrer speed required to achieve homogeneous suspension will result in the formation of aggregates, and thus it will affect the size and shape distributions of the crystals produced from the system.

The crystal growth rates from the open-loop simulations are calibrated with literature data,[32,37] and as a result, a set of values is chosen as follows: $(\phi/k_B, E_{pb}/k_B)_{110}$ = (1077.26K,227.10K), $(\phi/k_B, E_{pb}/k_B)_{101}$ = (800.66K,241.65K), and K_0^+ = 0.211/s. Furthermore, the moment models are used in the MPC scheme presented below in order to estimate the average shape of the crystal population with time. The accuracy of the moment models was verified through a comparison of the results with that obtained from the kMC simulations.[10,15]

MPC OF THE CRYSTAL SHAPE AND SIZE DISTRIBUTIONS

From the kMC simulation, we assumed that in situ measurements of the chord length distribution and crystal shape distribution (CSD) are available in real time and they are used to estimate the average aspect ratio $\langle\alpha\rangle = \langle h_{110}\rangle/\langle h_{101}\rangle$ over the next sampling time. Additionally, the uncertainty in the measurements (e.g., FBRM and PVM) is accounted for through the introduction of noise (fluctuation up to the 20% of the nominal value), and the measurements are obtained every Δ = 40 s.[15] We note that the computational time needed to solve the MPC problem using the moment model is only 0.12 s, and thus it is negligible compared to the sampling time (40 s). Furthermore, using the PBM based on the crystal volume distribution is more desirable because it requires fewer moment models to compute the evolution of the CSDs than those of the PBM based on the crystal heights in the direction of the (110) and (101) faces. Then, an optimal jacket temperature trajectory is computed by the MPC, driving the average shape of the entire crystal population to a desired set-point value.

Model Predictive Formulation. We propose an MPC design that minimizes the deviation of $\langle\alpha\rangle = \langle h_{110}\rangle/\langle h_{101}\rangle$ and G_{110}/G_{101} from a set point and penalizes the manipulated input values. In the objective function, we have included both the error in the aspect ratio and the ratio of growth rates in the direction of the (110) and (101) faces because the cost function helps the closed-loop system to be more robust toward disturbances such as model mismatch between the PBM and the reduced-order ODEs. Additionally, a set of weighting coefficients (w_1, w_2, w_3) are chosen by trial and error so that the controller is able to drive the crystallizer temperature to a desired value. In addition to the balance equations (eqs 4 and 5), we introduce additional practical constraints such as 4 °C ≤ T ≤ 25 °C in order to maintain the model protein in a proper condition. Furthermore, because of the presence of a limit in the actuator response time, the jacket temperature can be increased no faster than 2.0 °C/min. The resulting MPC is described as follows:

$$\begin{aligned}
&\underset{T_{j,1},\ldots,T_{j,i},\ldots,T_{j,p}}{\text{minimize}} \sum_{i=1}^{p} w_1\left(\frac{\langle\alpha(t_i)\rangle - \alpha_{set}}{\alpha_{set}}\right)^2 + w_2\left(\frac{\frac{G_{110}(\sigma(t_i))}{G_{101}(\sigma(t_i))} - \alpha_{set}}{\alpha_{set}}\right)^2 + w_3\left(\frac{T_{j,i+1} - T_{j,i}}{T_{j,i+1}}\right)^2\\
&\text{subject to } 4\ ^\circ\text{C} \le T_i \le 25\ ^\circ\text{C}\\
&\left|\frac{T_{j,i+1} - T_{j,i}}{\Delta}\right| \le 2\ ^\circ\text{C/min}\\
&G_{110}(\sigma) = 0.1843\sigma^3 - 1.1699\sigma^2 + 2.8885\sigma - 2.5616\\
&G_{101}(\sigma) = 0.1893\sigma^3 - 1.2264\sigma^2 + 2.9887\sigma - 2.5348\\
&\frac{dM_0}{dt} = B(\sigma) - \int_{V_p}^{\infty} \frac{n(V,t)}{\tau_p}\,dV - \int_0^{V_f} \frac{n(V,t)}{\tau_f}\,dV - \alpha_{eff}(M_0M_1 + 3M_{1/3}M_{2/3})\\
&\frac{dM_1}{dt} = G_{vol}M_0 - \int_{V_p}^{\infty} V\frac{n(V,t)}{\tau_p}\,dV - \int_0^{V_f} V\frac{n(V,t)}{\tau_f}\,dV\\
&\frac{dM_2}{dt} = 2G_{vol}M_1 - \int_{V_p}^{\infty} V^2\frac{n(V,t)}{\tau_p}\,dV - \int_0^{V_f} V^2\frac{n(V,t)}{\tau_f}\,dV + 2\alpha_{eff}(M_1M_2 + 3M_{4/3}M_{5/3})\\
&\frac{dC}{dt} = -\frac{\rho_c}{V_{MSMPR}}\frac{dM_1}{dt} + \frac{C_0}{\tau} + \frac{\rho_c}{V_{MSMPR}}\frac{d}{dt}\left(\int_0^{V_f} V\frac{n(V,t)}{\tau_f}\,dV\right) - \frac{C}{\tau}\\
&\frac{dT}{dt} = -\frac{\rho_c\Delta H_c}{\rho C_p V_{MSMPR}}\frac{dM_1}{dt} - \frac{U_cA_c}{\rho C_p V_{MSMPR}}(T - T_j) + \frac{T_{in} - T}{\tau}\\
&\frac{d\langle h_j\rangle}{dt} = G_j(\sigma) - \frac{B(\sigma)\,V_{MSMPR}\langle h_j(t)\rangle}{M_0(t)}\\
&\langle\alpha(t)\rangle \approx \frac{\langle h_{110}(t)\rangle}{\langle h_{101}(t)\rangle} \qquad \sigma = \ln(C/s)\\
&i = 1, 2, \ldots, p \quad \text{and} \quad j \in \{110,\ 101\}
\end{aligned} \quad (17)$$

where the prediction horizon is set as p = 10, $T_{j,i}$ is the jacket temperature at the time of the ith prediction step, and $t_i = t + i\Delta$. A set of new measurements are obtained at each sampling time, and subsequently a set of optimal jacket temperatures ($T_{j,1}$, $T_{j,2}$, ..., $T_{j,p}$) is obtained by solving eq 17. Then, the first

dx.doi.org/10.1021/ie5008163 | Ind. Eng. Chem. Res. 2014, 53, 15538−15548

value for the jacket temperature $T_{j,1}$ is applied to the crystallizer over the next sampling time. Furthermore, the interested reader may refer to refs 38 and 39 for further results regarding the design of robust control systems for crystallization processes.

CONTINUOUS CRYSTALLIZATION UNDER CLOSED-LOOP OPERATION

We used eq 3, which is only valid over the temperature range of 4−25 °C, to compute the solubility. As a result, the growth rate ratio $G_{110}(\sigma)/G_{101}(\sigma)$ varies from 0.7 to 1.12.[33] If the solubility equation is available for a higher temperature level, we can apply the kMC methodology to obtain a broader range for the growth rate ratio. Within this range, two set-point values, $\langle\alpha\rangle$ = 1.11 and 0.88, are chosen in which the former favors high supersaturation levels and the latter favors low supersaturation levels. Such a behavior that the crystal growth in a particular direction is favored by the supersaturation level is also verified through experiments by Durbin and Feher,[37] where they presented the relative growth rate between the (110) and (101) faces of the lysozyme crystals as a function of the supersaturation level. As discussed previously in this manuscript, conventional continuous crystallizers have usually been operated at large residence times and low supersaturation levels (i.e., metastable regime) to obtain large crystals and keep the nucleation rate low. Thus, this operating strategy results in a very low production rate. In order to achieve a high production rate at a low supersaturation level (i.e., metastable regime) and efficiently suppress a large number of crystals nucleated at a high supersaturation level (i.e., labile regime), we propose in this work an operating strategy taking advantage of the aggregation process through which we can accelerate the crystal growth and so the production rate.

However, direct manipulation of the stirrer speed in order to increase the aggregation rate during the operation is not desirable in practice because it may cause the crystallizer to move away from its steady state. Instead, we can indirectly control the aggregation rate by regulating the number concentration and size distribution of crystals inside the crystallizer because both variables affect the aggregation rate significantly.[10] Specifically, we studied the influence of varying the flow rates of the streams to the fines trap and product classification unit and the crystal cutoff sizes of those two processes. First, the flow rate of the stream to the fines trap is varied, as shown in Figures 3−6. When the residence time of the stream to the fines trap is decreased from τ_f = 180 to 72 s (i.e., the flow rate of the stream to the fines trap is increased), more small crystal fines are removed through the fines trap, thereby reducing the formation of aggregates (i.e., due to low number concentration), and thus the production rate is decreased by 31% from 2.5 × 10^{-5} to 1.8 × 10^{-5} cm^3/s (cf. Figure 5). For the simulation results of τ_f = 72 s, fewer crystal aggregates are formed while more small crystal fines are removed through the fines trap and, as a consequence, the average crystal size is increased (cf. Figure 6). On the other hand, if the residence time of the stream to the fines trap is increased from τ_f = 180 to 1800 s (i.e., the flow rate of the stream to the fines trap is decreased), more small crystals will stay in the crystallizer because the rate of the crystals removed through the fines trap is decreased. Furthermore, the high number concentration of the small crystal fines will promote the aggregation process so that more aggregates will be formed (cf. Figure 4). As a result, the production rate is increased by 16% from 2.5 × 10^{-5} to 2.9 × 10^{-5} cm^3/s. However, the

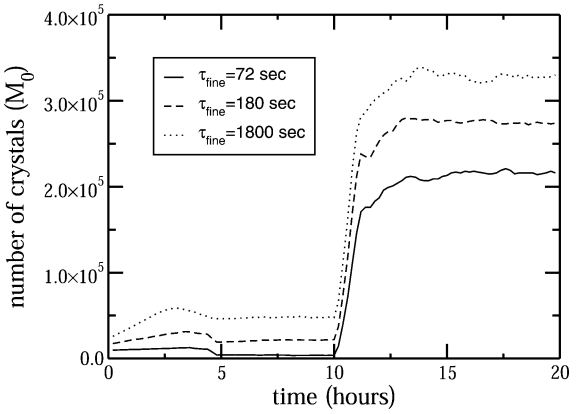

Figure 3. Dynamic evolution of the crystal number concentration (M_0) with time for varying the flow rate of the stream to the fines trap (τ_f = 72, 180, and 1800 s) under MPC for the desired set-point value, $\langle\alpha\rangle$ = 0.88. The set point is changed to $\langle\alpha\rangle$ = 1.11 after t = 10 h. The profiles are obtained by averaging 10 independent kMC simulations. The system parameters used in the simulations are as follows: τ_p = 180 s, V_f = 8 μm^3, and V_p = 5.12 × 10^5 μm^3.

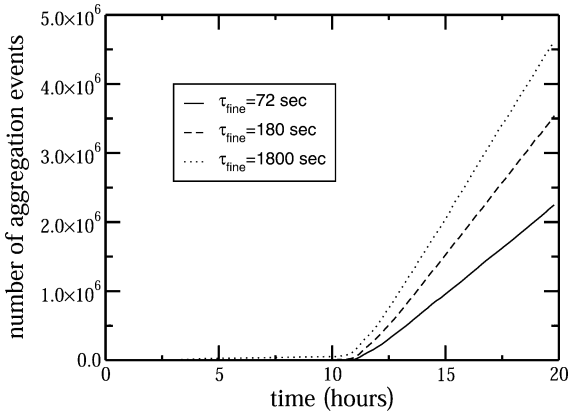

Figure 4. Dynamic evolution of the number of aggregation events taking place for varying the flow rate of the stream to the fines trap (τ_f = 72, 180, and 1800 s) under MPC for the desired set-point value, $\langle\alpha\rangle$ = 0.88. The set point is changed to $\langle\alpha\rangle$ = 1.11 after t = 10 h. The profiles are obtained by averaging 10 independent kMC simulations. The system parameters used in the simulations are as follows: τ_p = 180 s, V_f = 8 μm^3, and V_p = 5.12 × 10^5 μm^3.

average crystal size is decreased because the rate of accumulation of small crystals is slightly higher than the rate of formation of aggregates (cf. Figure 6). As shown in Table 3, increasing the residence time of the stream to the fines trap will increase the production rate because it will enforce small crystals to stay longer in the crystallizer and they will grow to a desired crystal size through aggregation and/or crystal growth. Therefore, we can achieve a higher production rate with fewer number of crystals with a desired size. Furthermore, the fines trap is needed to remove small crystal fines, so we suggest to use τ_f = 1800 s, which will result in the result very close to that of not using fines trap at all.

Additionally, it is shown in Figures 7 and 8 that using a product classifier unit with a greater cutoff size will cause the crystallizer to achieve a higher production rate. Specifically, when the cutoff size of the product classifier unit is increased from V_p = 6.4 × 10^4 to 5.1 × 10^5 μm^3, crystals stay in the crystallizer longer and more crystals are aggregated. As a result, the production rate is increased by 150% from 1.0 × 10^{-5} to 2.5

dx.doi.org/10.1021/ie5008163 | Ind. Eng. Chem. Res. 2014, 53, 15538−15548

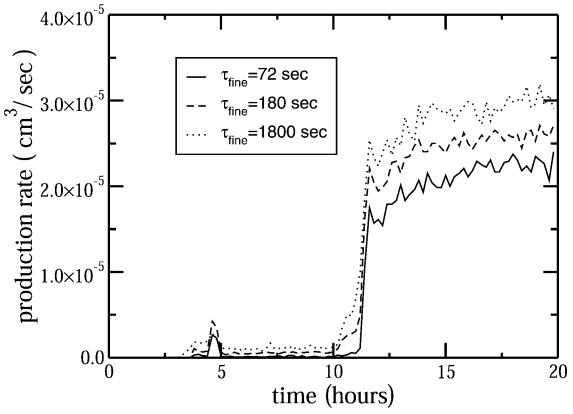

Figure 5. Dynamic evolution of the production rate of crystals for varying the flow rate of the stream to the fines trap (τ_f = 72, 180, and 1800 s) under MPC for the desired set-point value, $\langle\alpha\rangle$ = 0.88. The set point is changed to $\langle\alpha\rangle$ = 1.11 after t = 10 h. The profiles are obtained by averaging 10 independent kMC simulations. The system parameters used in the simulations are as follows: τ_p = 180 s, V_f = 8 μm^3, and V_p = 5.12 × 10^5 μm^3.

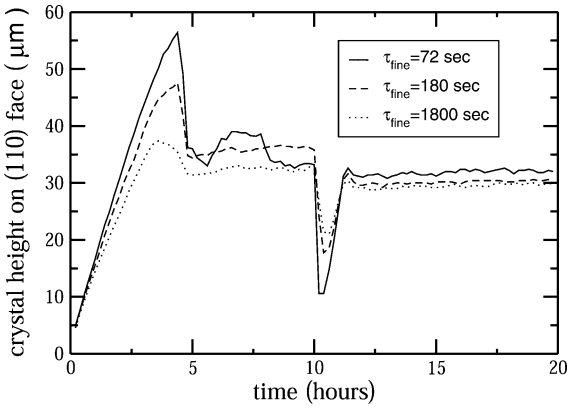

Figure 6. Dynamic evolution of the average crystal height in the direction of the (110) face for varying the flow rate of the stream to the fines trap (τ_f = 72, 180, and 1800 s) under MPC for the desired set-point value, $\langle\alpha\rangle$ = 0.88. The set point is changed to $\langle\alpha\rangle$ = 1.11 after t = 10 h. The profiles are obtained by averaging 10 independent kMC simulations. The system parameters used in the simulations are as follows: τ_p = 180 s, V_f = 8 μm^3, and V_p = 5.12 × 10^5 μm^3.

Table 3. Comparison of the Production Rates under Four Different Residence Times of the Stream to the Fines Trap after t = 15 h When the System Is at Steady State for the Set Point of $\langle\alpha\rangle$ = 1.11[a]

residence time, τ_f (s)	72	180	1800	∞
production rate (cm^3/s)	1.8 × 10^{-5}	2.5 × 10^{-5}	2.9 × 10^{-5}	3.1 × 10^{-5}

[a]Also, τ_f = ∞ implies the system without a fines trap process. The system parameters used in the simulations are as follows: τ_p = 180 s, V_f = 8 μm^3, and V_p = 5.12 × 10^5 μm^3.

× 10^{-5} cm^3/s. In Figure 9, the average crystal size is increased because of the formation of a number of crystal aggregates. Furthermore, increasing the flow rate of the product classifier will help the crystallizer to produce crystals with a narrower size distribution. From Figure 10, it is apparent that crystals with a very narrow size distribution are produced via implementation of the product classification unit with V_p = 5.12 × 10^5 μm^3. As

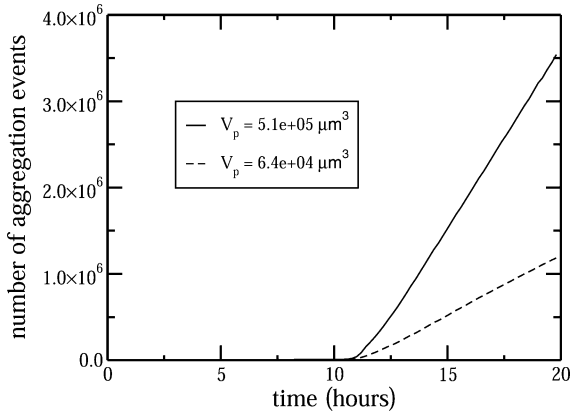

Figure 7. Dynamic evolution of the number of aggregation events taking place for varying the cutoff size for the product classification unit (V_p = 6.4 × 10^4 and 5.12 × 10^5 μm^3) under MPC for the desired set-point value, $\langle\alpha\rangle$ = 0.88. The profiles are obtained by averaging 10 independent kMC simulations. The set point is changed to $\langle\alpha\rangle$ = 1.11 after t = 10 h. The system parameters used in the simulations are as follows: τ_f = τ_p = 180 s and V_f = 8 μm^3.

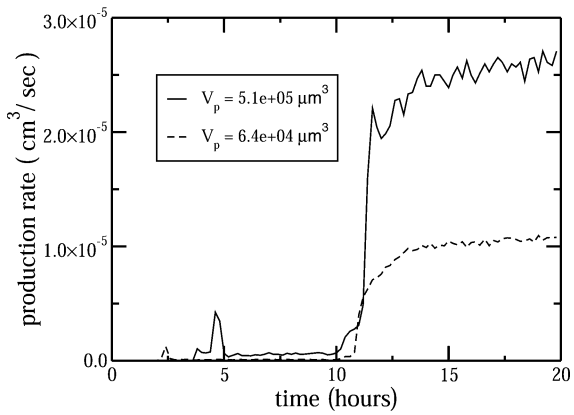

Figure 8. Dynamic evolution of the production rate of crystals for varying the cutoff size for the product classification unit (V_p = 6.4 × 10^4 and 5.12 × 10^5 μm^3) under MPC for the desired set-point value, $\langle\alpha\rangle$ = 0.88. The set point is changed to $\langle\alpha\rangle$ = 1.11 after t = 10 h. The profiles are obtained by averaging 10 independent kMC simulations. The system parameters used in the simulations are as follows: τ_f = τ_p = 180 s and V_f = 8 μm^3.

shown in Table 4, increasing the cutoff size of the product classification unit will increase the production rate because, for the same reason as before, it will essentially increase the residence time of small crystals, and those crystals will eventually leave the crystallizer with a desired size (i.e., a desired crystal volume).

Because a high supersaturation level is favored for the set point of $\langle\alpha\rangle$ = 1.11, the resulting high nucleation rate will increase the rate of accumulation of small crystals. Consequently, when the residence time of the stream to the fines trap is increased from τ_f = 72 to 1800 s, the average crystal size is decreased with a minor fluctuation. On the contrary, when a lower set-point value is desired, the nucleation rate is low, and as a result, the rate of accumulation of small crystals is sometimes lower and other times higher than the rate of formation of aggregates and thus shows a significant fluctuation, as shown in Figure 6.

The performance of the proposed MPC is presented in Figures 6−13. In Figure 11, the crystallizer temperature is

dx.doi.org/10.1021/ie5008163 | Ind. Eng. Chem. Res. 2014, 53, 15538−15548

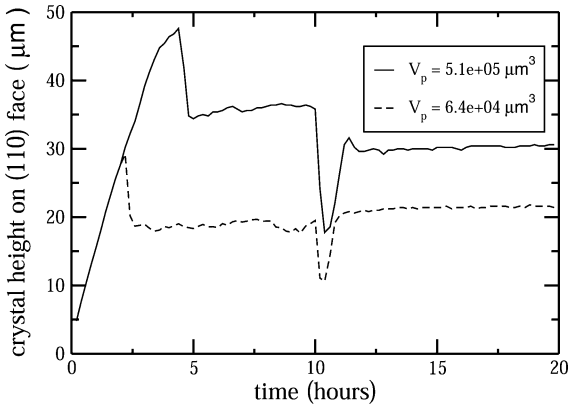

Figure 9. Dynamic evolution of the average crystal height in the direction of the (110) face for varying the cutoff size for the product classification unit (V_p = 6.4 × 10^4 and 5.12 × 10^5 μm^3) under MPC for the desired set-point value, $\langle\alpha\rangle$ = 0.88. The set point is changed to $\langle\alpha\rangle$ = 1.11 after t = 10 h. The profiles are obtained by averaging 10 independent kMC simulations. The system parameters used in the simulations are as follows: $\tau_f = \tau_p$ = 180 s and V_f = 8 μm^3.

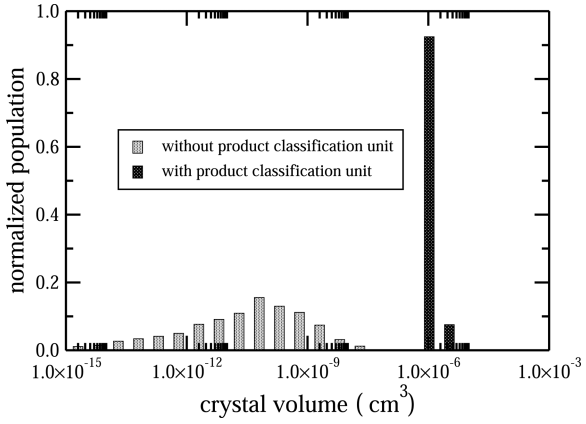

Figure 10. Normalized crystal volume distribution obtained from the closed-loop kMC simulations with and without a product classification unit under MPC at t = 19 h. The system parameters used in the simulations are as follows: $\tau_f = \tau_p$ = 180 s, V_f = 8 μm^3, and V_p = 5.12 × 10^5 μm^3.

Table 4. Comparison of the Production Rates under Three Different Cut-Off Sizes for the Product Classification Unit after t = 15 h When the System Is at Steady State for the Set Point of $\langle\alpha\rangle$ = 1.11[a]

cut-off size, V_p (μm^3)	0	6.4 × 10^4	5.1 × 10^5
production rate (cm^3/s)	7.0 × 10^{-8}	1.0 × 10^{-5}	2.5 × 10^{-5}

[a]Also, V_p = 0 implies a system without a product classification unit. The system parameters used in the simulations are as follows: $\tau_f = \tau_p$ = 180 s and V_f = 8μm3.

increased to the optimal value T = 23.6 °C and remains constant. The difference between the crystallizer and jacket temperatures at a steady state can be further reduced by using a material with a higher overall heat-transfer coefficient so that the higher heat-transfer rate is available and by setting the inflow temperature closer to the optimal temperature. Furthermore, we note that varying τ_f and τ_p does not affect the steady-state temperature (cf. eq 4). Furthermore, after t = 10 h, in order to test the performance of the system in response to set-point change, the desired crystal shape is changed from

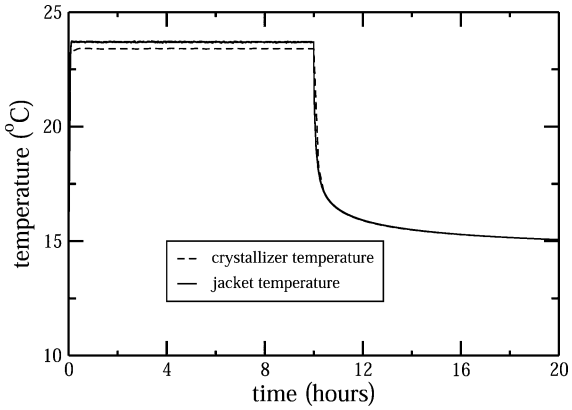

Figure 11. Dynamic evolution of the crystallizer temperature (T) and jacket temperature (T_j) with time under MPC for the desired set-point value, $\langle\alpha\rangle$ = 0.88. The set point is changed to $\langle\alpha\rangle$ = 1.11 after t = 10 h. The profiles are obtained by averaging 10 independent kMC simulations. The system parameters used in the simulations are as follows: $\tau_f = \tau_p$ = 180 s, V_f = 8 μm^3, and V_p = 5.12 × 10^5 μm^3.

$\langle\alpha\rangle$ = 0.88 to 1.11. As a consequence, the crystallizer temperature is decreased to T = 15.0 °C, which is the optimal temperature for the new set point, $\langle\alpha\rangle$ = 1.11. As presented in Figures 12 and 13, the proposed MPC was able to regulate the

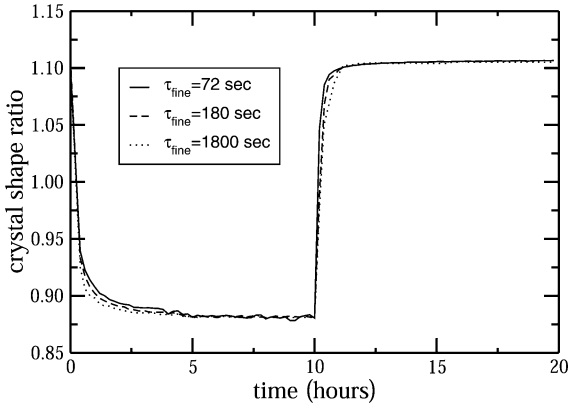

Figure 12. Dynamic evolution of the average shape $\langle\alpha\rangle$ of the entire crystal population with time for varying the flow rate of the stream to the fines trap (τ_f = 72, 180, and 1800 s) under MPC for the desired set-point value, $\langle\alpha\rangle$ = 0.88. The set point is changed to $\langle\alpha\rangle$ = 1.11 after t = 10 h. The profiles are obtained by averaging 10 independent kMC simulations. The system parameters used in the simulations are as follows: τ_p = 180 s, V_f = 8 μm^3, and V_p = 5.12 × 10^5 μm^3.

average shape of the crystal population to a desired value by appropriately handling the set-point change during the steady-state operation, the mismatch of moment models, and the uncertainty in the measurements. Additionally, when the residence time for the feed to the crystallizer is greater than 2 h, the solute concentration level drops more significantly owing to the production of larger crystals. Moreover, the response time of the system required to reach the steady state corresponding to the set point of $\langle\alpha\rangle$ = 0.88 is reduced because the aggregation process accelerates the crystal growth by merging two crystals into one larger aggregate. Specifically, it is indicated in Figures 4 and 12 that the system reaches its steady state earlier when there are more aggregates formed.

In conclusion, the aggregation process along with the product classification unit and fines trap helped to achieve a

dx.doi.org/10.1021/ie5008163 | Ind. Eng. Chem. Res. 2014, 53, 15538−15548

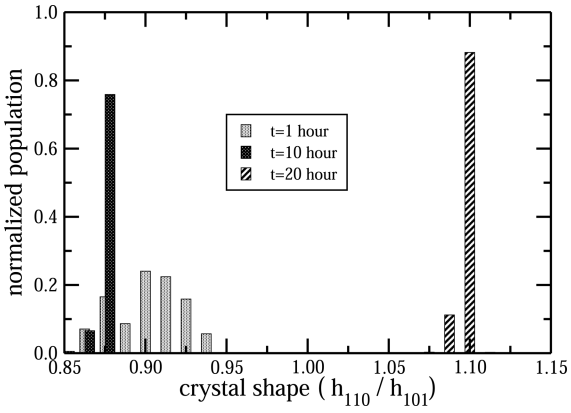

Figure 13. Normalized CSD at three different times during the simulation under MPC for the desired set-point value, $\langle\alpha\rangle = 0.86$. The set point is changed to $\langle\alpha\rangle = 1.11$ after $t = 10$ h. The histograms are obtained by averaging 10 independent kMC simulations, where the standard deviations for $t = 1$, 10, and 20 h are 0.02, 0.003, and 0.002, respectively. The system parameters used in the simulations are as follows: $\tau_f = \tau_p = 180$ s, $V_f = 8\ \mu m^3$, and $V_p = 5.12 \times 10^5\ \mu m^3$.

crystal population with a higher production rate and to reduce the response time required for the system to move from one steady state to another. In this work, we proposed a way to take advantage of the formation of aggregates through implementation of the product classification process and fines trap. As a result, the production of crystals with a high production rate as well as a low polydispersity is achieved. Furthermore, the proposed MPC scheme can successfully drive the average shape of the crystal population to desired shape distributions, suppressing the effect of disturbances. The control action can be more aggressive by using a higher actuator limit on the manipulated input (i.e., jacket temperature), which will, in turn, result in a better controller performance.

CONCLUSIONS

In this work, the minimum stirrer speed required to maintain the crystals in a homogeneous suspension resulted in the formation of aggregates, and a fines trap and a product classification unit were implemented to indirectly control the degree of formation of crystal aggregation. To this end, we first modeled the fines trap and product classification unit as well as the nucleation, crystal growth, and aggregation in a continuous crystallization process through kMC simulations. Furthermore, the performance in terms of regulating the degree of the aggregation process was studied by varying the flow rate of the stream to the fines trap and using different cutoff sizes for the product classification unit. Specifically, the production rate is increased by 61% from 1.8×10^{-5} to 2.9×10^{-5} cm^3/s when the residence time of the stream to the fines trap is increased, from $\tau_f = 72$ to 1800 s, and the production is increased by 150%, from 1.0×10^{-5} to 2.5×10^{-5} cm^3/s, when the cutoff size of the product classifier unit is increased from $V_p = 6.4 \times 10^4$ to $5.1 \times 10^5\ \mu m^3$. Additionally, moment models were derived to approximate the evolution of the crystal volume distribution with time in the continuous crystallization process, and they were used in order to design an MPC.

As a result, a very narrow size distribution was obtained at the steady state because of implementation of the product classifier. Furthermore, the average shape of the crystal population was successfully regulated to a desired distribution by a proposed MPC through manipulation of the jacket temperature. By using a low flow rate to the fines trap (i.e., high τ_f), which will, in turn, promote the formation of aggregates, the response time of the system toward the desired crystal shape set point is reduced and the crystal production rate is increased. Moreover, using a material with a high overall heat-transfer coefficient for the crystallizer wall and a higher actuator limit will allow for the jacket temperature to take a more prompt action and reach its optimal value faster.

AUTHOR INFORMATION

Corresponding Author

*E-mail: pdc@seas.ucla.edu.

Notes

The authors declare no competing financial interest.

ACKNOWLEDGMENTS

Financial support from the National Science Foundation (NSF; Grant CBET-0967291) and the Extreme Science and Engineering Discovery Environment (Grant TG-CCR120003), as well as the NSF Graduate Research Fellowship DGE-0707424 given to M.N., is gratefully acknowledged.

REFERENCES

(1) Griffin, D. W.; Mellichamp, D. A.; Doherty, M. F. Reducing the mean size of API crystals by continuous manufacturing with product classification and reycle. *Chem. Eng. Sci.* **2010**, *65*, 5770−5780.

(2) Alvarez, A.; Singh, A.; Myerson, A. S. Crystallization of cyclosporine in a multistage continuous MSMPR crystallizer. *Cryst. Growth Des.* **2011**, *11*, 4392−4400.

(3) Majumder, A.; Nagy, Z. Fines removal in a continuous plug flow crystallizer by optimal spatial temeprature profiles with controlled dissolution. *AIChE J.* **2013**, *59*, 4582−4594.

(4) Zwietering, T. N. Suspending of solid particles in liquid by agitators. *Chem. Eng. Sci.* **1958**, *8*, 244−253.

(5) Kolar, V. Studies on mixing: suspending solid particles in liquids by means of mechanical agitation. *Collect. Czech. Chem. Commun.* **1961**, *26*, 613−627.

(6) Harnby, N., Edwards, M. F., Nienow, A. W., Eds. *Mixing in the process industries*; Academic Press: New York, 1992.

(7) Baldi, G.; Conti, R.; Alaria, E. Complete suspension of particles in mechanically agitated vessels. *Chem. Eng. Sci.* **1978**, *33*, 21−25.

(8) Nienow, A. W. Suspension of solid particles in turbin agitated baffled vessels. *Chem. Eng. Sci.* **1968**, *23*, 1453−1459.

(9) Nicholas, C. S.; Reginald, B. H. CFD simulation of solids suspension in mixing vessels. *Can. J. Chem. Eng.* **2002**, *80*, 1−6.

(10) Kwon, J. S.; Nayhouse, M.; Christofides, P. D.; Orkoulas, G. Modeling and control of shape distribution of protein crystal aggregates. *Chem. Eng. Sci.* **2013b**, *104*, 484−497.

(11) Christofides, P. D.; Armaou, A.; Lou, Y.; Varshney, A. *Control and Optimization of Multiscale Process Systems*; Birkhäuser: Boston, 2008.

(12) Durbin, S. D.; Feher, G. Simulation of lysozyme crystal growth by the Monte Carlo method. *J. Cryst. Growth* **1991**, *110*, 41−51.

(13) Chiu, T.; Christofides, P. D. Nonlinear control of particulate processes. *AIChE J.* **1999**, *45*, 1279−1297.

(14) El-Farra, N. H.; Chiu, T.; Christofides, P. D. Analysis and control of particulate processes with input constraints. *AIChE J.* **2001**, *47*, 1849−1865.

(15) Kwon, J. S.; Nayhouse, M.; Christofides, P. D.; Orkoulas, G. Modeling and control of crystal shape in continuous protein crystallization. *Chem. Eng. Sci.* **2014a**, *107*, 47−57.

(16) Pathath, P. K.; Kienle, A. Nonlinear oscillations in ammonium sulfate crystallization: a comparison of different model predictions. *Ind. Eng. Chem. Res.* **2003**, *42*, 6949−6955.

(17) Smejkal, B.; Helk, B.; Rondeau, J.; Anton, S.; Wilke, A.; Scheyerer, P.; Fries, J.; Hekmat, D.; Weuster-Botz, D. Protein

crystallization in stirred systems-scale-up via the maximum local energy dissipation. *Biotechnol. Bioeng.* **2013**, *110*, 1956−1963.
(18) Tait, S.; White, E.; Litster, J. A study on nucleation for protein crystallization in mized vessels. *Cryst. Growth Des.* **2009**, *9*, 2198−2206.
(19) Nanev, C. N.; Tsekova, D. Heterogeneous nucleation of Hen-Egg-White Lysozyme-Molecular approach. *Cryst. Res. Technol.* **2000**, *35*, 189−195.
(20) Suzuki, Y.; Miyashita, S.; Komatsu, H.; Sato, K.; Yagi, T. Crystal growth of Hen Egg White Lysozyme under high pressure. *Jpn. J. Appl. Phys.* **1994**, *33*, 1568−1570.
(21) Galkin, O.; Vekilov, P. G. Nulceation of protein crystals: critical nuclei, phase behavior, and control pathways. *J. Cryst. Growth* **2001**, *232*, 63−76.
(22) Cacioppo, E.; Munson, S.; Pusey, M. L. Protein solubilities determined by a rapid technique and modification of that technique to a micro-method. *J. Cryst. Growth* **1991**, *110*, 66−71.
(23) Cacioppo, E.; Pusey, M. L. The solubility of the tetragonal form of hen egg white lysozyme from pH 4.0 to 5.4. *J. Cryst. Growth* **1991**, *114*, 286−292.
(24) Shi, D.; Mhaskar, P.; El-Farra, N. H.; Christofides, P. D. Predictive control of crystal size distribution in protein crystallization. *Nanotechnology* **2005**, *16*, S562−S574.
(25) Ke, S. C.; DeLucas, L. J.; Harrison, J. G. Computer simulation of protein crystal growth using aggregates as the growth unit. *J. Phys. D: Appl. Phys.* **1998**, *31*, 1064−1070.
(26) Aldabaibeh, N.; Jones, M. J.; Myerson, A. S.; Ulrich, J. The solubility of orthorhombic lysozyme chloride crystals obtained at high pH. *Cryst. Growth Des.* **2009**, *9*, 3313−3317.
(27) Weber, M.; Jones, M.; Ulrich, J. Crystallization as a purification method for jack bean urease: on the suitability of poly(ethylene), Li_2SO_4 and NaCl as precipitants. *Cryst. Growth Des.* **2008**, *8*, 711−716.
(28) Müller, C.; Liu, Y.; Migge, A.; Pietzsch, M.; Ulrich, J. Recombinant L-Asparaginase B and its Crystallization—What is the Nature of Protein Crystals? *Chem. Eng. Technol.* **2011**, *34*, 571−577.
(29) Müller, C.; Ulrich, J. A more clear insight of the lysozyme crystal composition. *Cryst. Res. Technol.* **2011**, *46*, 646−650.
(30) Nayhouse, M.; Kwon, J. S.; Christofides, P. D.; Orkoulas, G. Crystal Shape Modeling and Control in Protein Crystal Growth. *Chem. Eng. Sci.* **2013**, *87*, 216−223.
(31) Levenspiel, O. *Chemical Reaction Engineering*; Wiley Eastern: New Delhi, India1998.
(32) Kwon, J. S.; Nayhouse, M.; Christofides, P. D.; Orkoulas, G. Modeling and control of protein crystal shape and size in batch crystallization. *AIChE J.* **2013a**, *59*, 2317−2327.
(33) Kwon, J. S.; Nayhouse, M.; Christofides, P. D.; Orkoulas, G. Protein cyrstal shape and size control in batch crystallization: Comparing model predictive control with conventional operating policies. *Ind. Eng. Chem. Res.* **2014b**, *53*, 5002−5014.
(34) Asiri, S. Design and implementation of differential agitators to maximize agitating performance. *Int. J. Mech. Appl.* **2012**, *2*, 98−112.
(35) Guiraud, P.; Costes, J.; Bertrand, J. Local measurements of fluid and particle velocities in a stirred suspension. *Chem. Eng. J.* **1997**, *68*, 75−86.
(36) Paul, E.; Atiemo-Obeng, V.; Kresta, S. *Handbook of industrial mixing*; Wiley: New York, 2003.
(37) Durbin, S. D.; Feher, G. Crystal growth studies of lysozyme as a model for protein crystallization. *J. Cryst. Growth* **1986**, *76*, 583−592.
(38) Shi, D.; El-Farra, N. H.; Li, M.; Mhaskar, P.; Christofides, P. D. Predictive control of particle size distribution in particulate processes. *Chem. Eng. Sci.* **2006**, *61*, 268−281.
(39) Chiu, T.; Christofides, P. D. Robust Control of Particulate Processes Using Uncertain Population Balances. *AIChE J.* **2000**, *46*, 266−280.